Acta metall. Vol. 36, No. 4, pp. 1085–1098, 1988
Printed in Great Britain.

0001-6160/88 $3.00 + 0.00

MARTENSITIC TRANSFORMATION INDUCED BY A TENSILE STRESS PULSE IN Fe–22.5 wt% Ni–4 wt% Mn ALLOY

SOON-NAM CHANG[1]† and MARC ANDRÉ MEYERS[2]

[1]Department of Applied Mechanics and Engineering Science, University of California at San Diego, La Jolla, California, U.S.A.

[2]Department of Materials and Metallurgical Engineering, and Center for Explosives Technology Research, New Mexico Institute of Mining and Technology, Socorro, NM 87801, U.S.A.

(*Received* 21 *April* 1987)

Abstract—The kinetics of martensitic transformation induced by a tensile pulse, produced by shock-wave reflection at the rear free surfaces of both projectile and target, has been investigated. The tensile stress thus generated prevails in time durations of microseconds and fractions thereof, and produces a considerable increase in the magnitude of the driving force for the $\gamma \rightarrow \alpha'$ martensitic transformation. This tensile-pulse technique allows the determination of kinetic and thermodynamic parameters (driving forces and activation energies for transformation) in regimes not attainable by conventional techniques. This work is a natural extension of Thadhani and Meyers' [*Acta metall.* **34,** 1625 (1986)] investigation. While Thadhani and Meyers investigated an alloy exhibiting burst characeristics, the alloy chosen for this investigation (Fe–22.5 wt% Ni–4 wt% Mn) exhibits a very sluggish isothermal transformation. It was found that the volume fraction of martensite transformed at a constant impact pressure increased with *increasing* pulse duration at a constant temperature, and with decreasing temperature (−60 to −177°C) at a constant pulse duration. The C-curve kinetic behavior that is typical of isothermal martensitic transformations was not observed. From the results obtained, the isothermal kinetics and energetics of the martensitic transformation were obtained and interpreted in terms of the existing theories. The activation volume for nucleation was found to be equal to 65 atomic volumes. The morphology of martensite under zero stress was observed to consist of many fragmented plates of the same orientation, while the martensite transformed under impact conditions was more often lenticular. Transmission electron microscopy and diffraction analysis were made on martensite induced by the tensile pulse technique, and the martensite habit plane was found to be $(112)_f$.

Résumé—Nous avons étudié la cinétique de la transformation martensitique induite par une impulsion de contrainte en traction produite par la réflexion d'ondes de choc sur les surfaces libres arrières du projectile et de la cible. La contrainte de traction ainsi créée agit pendant des temps de l'ordre de quelques microsecondes et fractions de microsecondes; elle provoque un accroissement considérable de la force motrice de la transformation martensitique $\gamma \rightarrow \alpha'$. Cette technique permet de déterminer les paramètres cinétiques et thermodynamiques (forces motrices et énergies d'activation de la transformation) dans des régimes que l'on ne pouvait pas atteindre par les techniques classiques. Ce travail fait suite aux travaux de Thadhani et de Meyers [*Acta metall.* **34,** 1625 (1986)]. Alors que ces derniers avaient étudié un alliage présentant des caractéristiques brutales, l'alliage que nous avons choisi pour notre étude (Fe–22,5% pond. Ni–4% pond. Mn) présente une transformation isotherme très lente. Nous avons trouvé que la fraction volumique de martensite transformée, pour une pression d'impact constante, croît pour une durée d'impulsion croissante à température constante, et pour une température décroissante (−60 à −177°C) pour une durée d'impulsion constante. Nous n'avons pas observé le comportement cinétique en courbe C typique des transformations martensitiques isothermes. Nous avons déduit de nos résultats les caractéristiques cinétiques et énergétiques isothermes de la transformation martensitique, et nous les avons interprétées en fonction des théories actuelles. Nous avons trouvé un volume d'activation de la germination égal à 65 volumes atomiques. La morphologie de la martensite sous contrainte nulle consiste en de nombreuses plaquettes fragmentées de même orientation, alors que la martensite transformée sous impact est plus souvent lenticulaire. Nous avons analysé par macroscopie et diffraction électroniques en transmission la martensite créée par la technique des impulsions de contrainte; nous avons trouvé comme plan d'accolement de la martensite le plan $(112)_f$.

Zusammenfassung—Die Kinetik der durch eine pulsförmige Zugbelastung induzierten martensitischen Umwandlung wurde untersucht. Die Pulse wurden durch Reflexion einer Schockwelle an der freien Rückseite sowohl von Projektil als auch Zielfläche erzeugt. Der Zugspannungspuls dauert einige Mikrosekunden oder auch nur einen Bruchteil davon und stellt eine beträchtliche Erhöhung der treibenden Kraft für die martensitische Umwandlung $\gamma \rightarrow \alpha'$ dar. Aus diesem Experiment mit Zugspannungspulsen lassen sich die kinetischen und thermodynamischen Parameter (treibende Kräfte und Aktivierungsenergien der Umwandlung) für Bedingungen bestimmen, die mit herkömmlichen Verfahren experimentell nicht erreichbar sind. Diese Arbeit stellt eine konsequente Erweiterung der Arbeit von Thadani und Meyers [*Acta metall.* **34,** 1625 (1986)] untersuchten eine Legierung, die durch plötzliche

†Work done in partial fulfillment of the degree of Doctor of Philosophy at New Mexico Institute of Mining and Technology.

Umwandlungen charakterisiert ist; die vorliegende Arbeit erweitert die Untersuchungen auf die Legierung Fe–22,5 Gew.-% Ni–4 Gew.-% Min, welche durch eine sehr träge isotherme Umwandlung ausgezeichnet ist.

Der Volumanteil des umgewandelten Martensits bei konstantem Aufschlagdruck nimmt in dieser Legierung mit der Pulslänge bei konstanter Temperatur und mit abnehmender Temperatur (−60 bis −177°C) bei konstanter Pulslänge zu. Das kinetische Verhalten der C-Kurve, welches für isotherme martensitische Umwandlungen typisch ist, wurde nicht beobachtet. Aus den erhaltenen Ergebnissen wurden die isotherme Kinetik und die energetischen Aspekte der martensitischen Umwandlung abgeleitet und mit vorhandenen Theorien gedeutet. Das Aktivierungsvolumen der Keimbildung ergibt sich zu 65 Atomvolumina. Die Morphologie des Martensits unter der Spannung Null besteht aus vielen fragmentierten Platten derselben Orientierung, wohingegen der unter Pulslast gebildete oft linsenförmig war. Der durch Zugspannungspulse erzeugte Martensit wurde im Elektronenmikroskop untersucht; als Habitebene ergab sich $(112)_f$.

1. INTRODUCTION

Externally applied stresses can increase or decrease the driving force for martensitic transformation [2–5]. It is well known [5] that, while uniaxial tension (or compression) stresses stimulate the transformation, hydrostatic compression stresses suppress it.

Several invetigators observed that there was no martensite found in Fe–Ni–C alloys upon shock compression. However, in similar alloys, Meyers and Guimaraes [6] and Snell *et al.* [7] were able to find martensite transformation above the M_s, induced by a tensile pulse generated by the reflection of a shock wave at a free surface. Recently, Thadhani and Meyers [1] systematically investigated the burst martensitic transformation in Fe–32 wt% Ni–0.035 wt% C alloy induced by a tensile stress pulse, using a one-stage gas-gun; they showed that burst transformation was in effect a very rapid isothermal transformation. The present work is a natural extension of their experiments [1], with an alloy, Fe–22.5 wt% Ni–4 wt% Mn, exhibiting radically different transformation kinetics. While Fe–32 wt% Ni–0.035 wt% C exhibits burst characteristics, Fe–22.5 wt% Ni–4 wt% Mn has such sluggish transformation kinetics that exposure of 1 hr at −120°C (the nose of the C-curve) is required for the first perceptible transformation signs. This alloy was previously investigated by Korenko and Cohen [8, 9], who used high magnetic fields to increase the driving force for the transformation; they were able to obtain the transformation kinetics and found that the maximum transformation rate obtained at −120°C. They analyzed the C-curve kinetic behavior and obtained activation energies and driving forces for the transformation.

The objectives of the investigation whose results are presented here were (a) to use the tensile pulse technique to obtain fundamental kinetic and thermodynamic parameters for this alloy and (b) to compare these parameters with other alloys in an attempt to identify unifying features.

2. EXPERIMENTAL PROCEDURES

An alloy with composition Fe–22.5 wt% Ni–4.0 wt% Mn was provided in the form of a hot-rolled slab by G. B. Olson, MIT. The alloy was originally cast at the U.S. Steel Laboratory for Fundamental Research in the form of an 8 kg cylindrical ingot and hot-rolled into slabs with intermediate anneals at 1200°C.

The slab was homogenized at 1300°C for 72 h in a vacuum furnace at 2×10^{-5} torr and hot-rolled to obtain desired thicknesses at 10.4, 4.8 and 3.5 mm by successive passes through the rolling mill. Prior to each rolling, the slab was heated to 1000°C for 15 min in a positive pressure argon atmosphere. The specimens were machined from the hot-rolled plates into 30 mm diameter circular discs for the target sample. Final thickness of each specimen was achieved by mechanical grinding of both faces, to prevent surface compositional complications. In order to alleviate discrepancies in grain sizes, the disc samples were heat treated at 1100°C for 20 min and air cooled. This treatment was acccomplished by placing the discs in Sen-Pak foil bags, preventing oxidation of the surface. After the treatment, the grain size (measured by the linear intercept technique) was found to be 81 μm in all samples.

The disc-shaped specimens were mounted in AISI 304 stainless steel rings and held in place by 7° taper on the inner circumference of the ring. Figure 1 is a schematic representation of the target specimen. The ring plays a role in minimizing the effects of converging release waves.

The flyer plate thickness in these impact experiments was always maintained half of that of the corresponding targets in order to ensure a tensile pulse in the center of the target for the alloy system employed. The diameter of the flyer plates was 56 mm. The thickness and diameter of the flyer plate as well as its material properties, along with the impact velocity of the flyer plate, control the shape of the tensile pulse. In all experiments 6061-T6 aluminum alloy flyer plates were used. The projectile travelling through the evacuated gun barrel was keyed and had an O-ring seal. The head of the projectile consisted of a flyer plate backed up by honeycomb and was accelerated in the gun barrel by the highly compressed gas. The impact experiments were conducted at SRI-International with a 63.5 mm diameter one-stage gas gun. The procedure for using

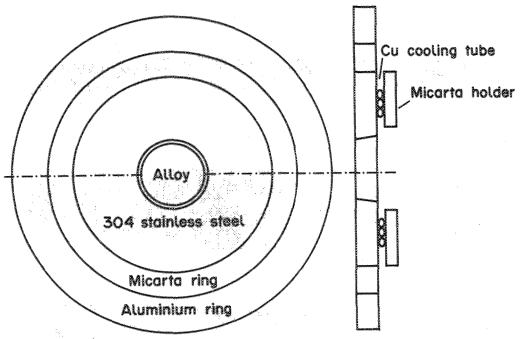

Fig. 1. Schematic representation of target design.

the fully instrumented gas gun was similar to that of Thadhani [10] who described it in detail. Figure 2 is the schematic representation of the target and the accelerating projectile within the gas gun.

The specimens recovered from the gas gun impact experiments were cut in a direction normal to the impact surface, in order to analyze the morphology and characteristics of the transformed martensite. For optical microscopy, the specimens were mechanically polished by conventional methods and then chemically polished in an agitating 65% H_2O_2, 30% H_2O, and 5% HF solution for 4 s at room temperature. This was followed by etching in 2 g $NaHSO_4$ with 100 ml H_2O for 30 s. Using this polishing method the martensite morphology, as well as austenitic grain boundaries and twin boundaries, were clearly revealed.

Specimens for transmission electron microscopy were cut by diamond blade to 1 mm thickness, and ground with 600 grit SiC strip to the thickness of 0.4 mm; this was followed by chemical polishing to less than 0.2 mm thickness. Disks of 3 mm diameter were punched (from the transformation area indicated by optical micrography of these specimens), jet-polished and perforated by using an electrolyte consisting of 100 g Na_2CrO_4–$4H_2O$ and 500 ml glacial acetic acid, at 70–80 V (DC) and at room temperature.

A point counting techniquie [11] was employed to determine the volume fraction of martensite transformed. In this technique fifteen micrographs (at a magnification of $\times 900$) were taken from the maximum pulse duration zone across the cross section of each specimen, and were superimposed on transparent square grids (number of intersection points: 1120). The fraction of point-intersections falling on the martensite was computed as compared to the points falling on the austenitic phase and the grain/twin boundaries. The counting was executed in three random orientations on each photomicrograph and the results averaged. The maximum transformation zone was considered to correspond to the position of maximum tensile pulse duration in each shock-loaded specimen.

The mean volume per martensite plate ($\bar{V}$) as a function of the volume fraction transformed (f) was determined by using Fullman's equation [12] for an aggregate of circular discs. These values were measured from optical micrographs taken at $\times 740$ in a $17 \times 25\,cm^2$ area. From these measurements and the volume fraction (f) estimated as mentioned previously the mean volume per martensite plate was determined.

For habit plane determination, a numerical computer calculation recently proposed [13] was adapted. The surface normal of each austenitic grain where martensite plates exist was determined from four different directions of slip lines of the {1 1 1} plane produced by micro-Vickers indentations. A similar calculation was independently performed to determine the surface normal from angles between habit planes of martensite plates transformed on the same grain. The family of the habit planes was assumed to be of an arbitrary type. When the surface normals of the grain from both calculations were equal, the arbitrarily given type of habit plane was identified. In order to confirm the habit plane determined by this method, transmission electron microscopy and diffraction analysis were made on martensite induced by the tensile pulse.

3. RESULTS AND DISCUSSION

A set of preliminary experiments was conducted with two objectives:

(1) To determine whether stress-induced martensite

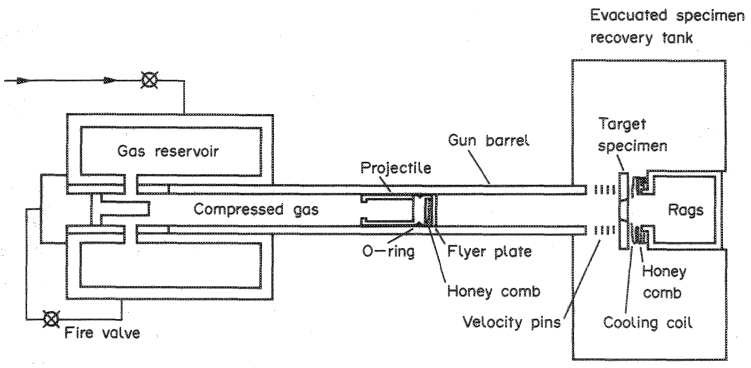

Fig. 2. Schematic representation of gas-gun showing target and projectile.

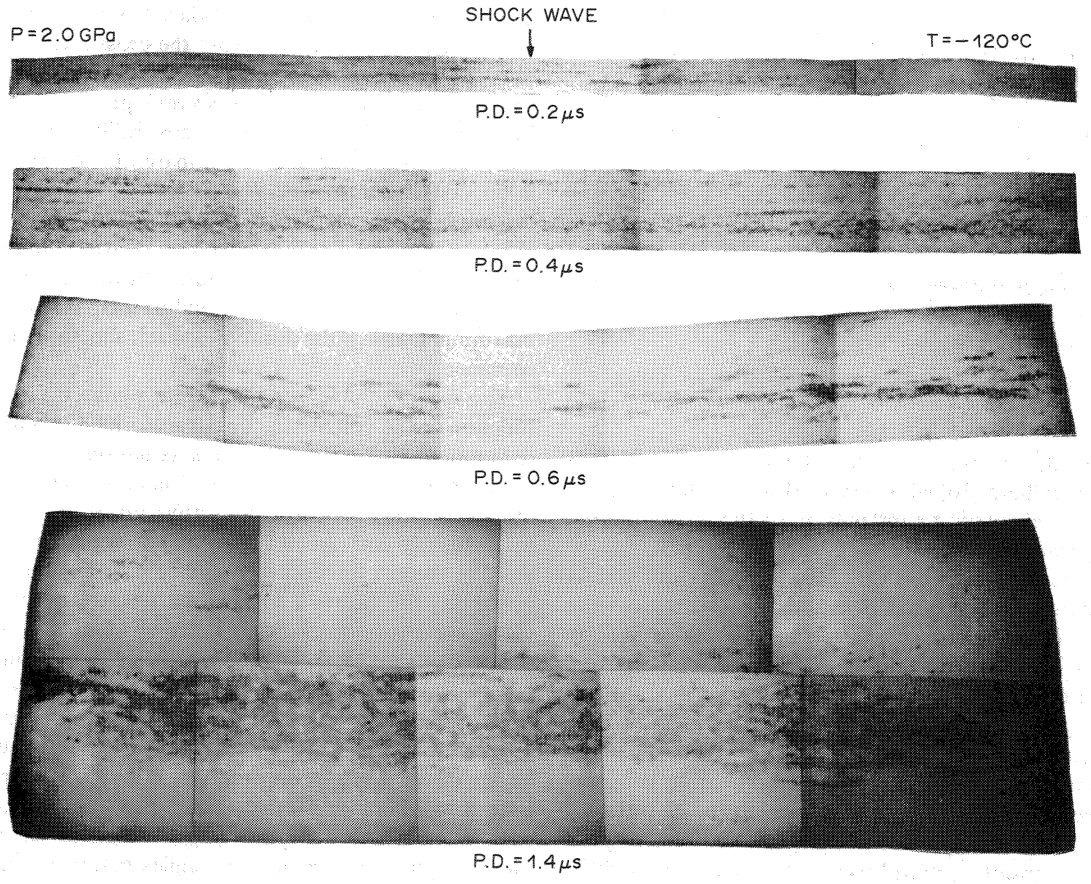

Fig. 3. Micrographs of cross-sections of recovered specimens impacted at −120°C and 2 GPa, with varying pulse duration.

could be formed by a tensile pulse of sub-microsecond duration in Fe–22.5% Ni–4% Mn alloy, which was isothermally transformed under no stress conditions by holding at −196°C for times longer than 70 min. The answer to this is that stress-induced martensite does occur.

(2) To determine what kind of stress (tensile or compressive) can provide sufficient driving force for the martensitic transformation. It was shown that shock compressive stresses, of which maximum pressure duration is at the impact surface, did not induce the martensitic transformation in this alloy, but in fact the tensile stresses did. The evidence is simply illustrated by the transformation zone as seen at cross sections of the impacted target specimens. The martensite was not formed in the zones submitted exclusively to the compressive wave, but in the localized areas where the tensile pulse was of a maximum amplitude and duration.

The preliminary experiments were conducted at pressures of 1.7, 2.0, 2.5 and 3.2 GPa and temperature of −100°C. At the impact pressure of 2.0 GPa, corresponding to the impact velocity of 200 m/s, martensite was observed with a minimum fraction of spalling. This pressure condition was used in all of the subsequent experiments.

The one-dimensional SWAP-7[14] and SIN [15] codes were used to obtain pressure histories with the impacted samples. The density and the equation of state terms for Fe–22.5% Ni–4% Mn are important parameters for operating both computer codes. The density of the alloy is given as a function of temperature [8]: $8.148–1.96 \times 10^{-4} T(°C)$ (g/cm^3). Since the Hugoniot relationships for the alloy were not available, the values of the sound velocity, $C_0 (=4.37$ km/s) and the constant, $S(=1.73)$ for Fe–26.2% Ni [16] were used.

A summary of gas-gun operating conditions and impact results is given in Table 1.

3.1. Experiments with varying durations and temperatures

The important objective in this investigation was to study the kinetics of martensitic transformation in the Fe–22.5% Ni–4% Mn alloy. In order to achieve this purpose it was necessary to explore whether the fraction of martensite transformed would change with varying tensile pulse duration, at various temperatures and constant stress. The shock impact experiments were conducted at a constant pressure of 2 GPa, and as a function of temperature (−60 to −177°C) for tensile pulse durations of 0.2, 0.4, 0.6 and 1.4 μs.

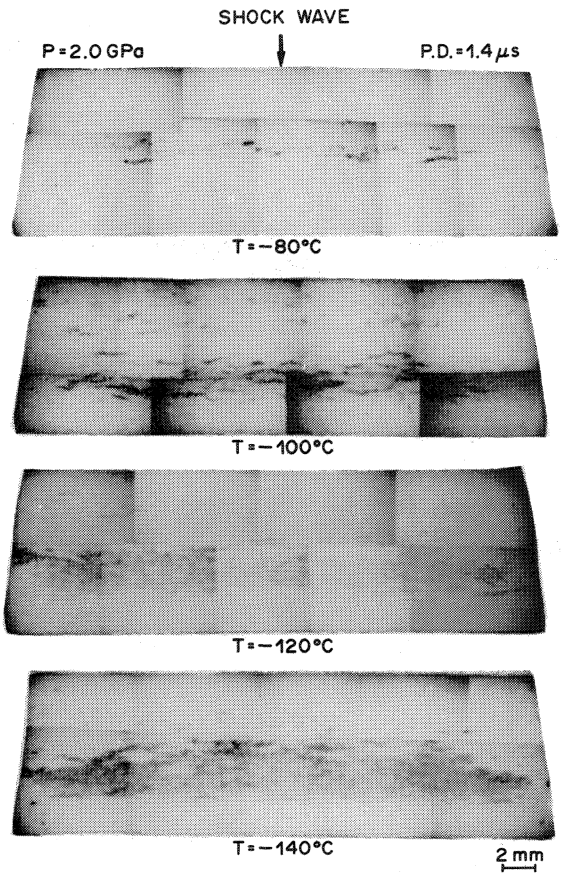

Fig. 4. Micrographs of cross-sections of recovered specimens impacted at varying temperatures with constant pulse duration of 1.4 μs.

The micrographs of cross sections of specimens impacted at varying pulse durations at constant stress, 2 GPa, and temperature, −120°C, are shown in Fig. 3. The transformed martensite was obtained as black striations resulting from an etching action. This transformation product is localized slightly towards the rear of the center in the target specimens.

Figure 4 shows the micrographs of the cross sections of specimens impacted at varying temperatures, but with constant pulse duration. The amount of transformation is observed to increase with decrease in the impact temperature. This characteristic of the transformation behavior appears to be similar in all series of the impact experiments. The volume fraction of martensite transformed in each specimen was computed at the position of maximum tensile pulse duration.

The transformed martensite along striations appears to form nearly perpendicular to the shock wave propagation direction. These striations are not consistently connected to each other within the zone of maximum pulse duration as illustrated in Fig. 5. This can be attributed to either discontinuous interactions of two release waves from both back free surfaces of the target and the flyer plate, or effects of the inhomogeneously distributed chemical composition in the alloy. To verify the latter hypothesis, an electron probe microanalysis was conducted along the dotted line across the martensite cluster, as indicated in Fig. 6(a). The results of Fig. 6(b) show that there are no significant variations in the chemical content of Mn or Ni between transformed and untransformed zone. Another area was also scanned in a similar way, but no variations of components were found. It is therefore concluded that the elements are uniformly distributed in the alloy. Conversely, the discontinuous interactions of two release waves appear to be the probable cause for these phenomena on a microscopic scale. This effect may be interrelated with the intrinsic instabilities due to localized nonhomogeneous deformation in compressive shock waves [17] and/or the instability phenomena of dynamic tensile pulse interactions [18].

3.2. *Quantitative metallography*

The quantitative values of average volume of a martensite plate were measured by Fullman's method [12]. Figure 7 shows the variation of the average volume of a martensite plate as a function of the fraction transformed. It was observed that the mean volume per martensite plate ($\bar{V}$) is not sensitive to the volume fraction of martensite transformed by the application of a tensile pulse of varying durations. Pati and Cohen [19] observed in Fe–Ni–Mn alloys that the values of $\bar{V}$ were in the range of 1.0–4.0 × 10^{-10} cm^3 until 30% martensite transformed. Korenko [8] reported that $\bar{V}$ remains constant (3 × 10^{-8} cm^3) over the range of 7–35% martensite. An average volume, $\bar{V}$, in this investigation was 1.27 × 10^{-9} cm^3.

3.3. *Kinetics and energetics*

3.3.1. Kinetics. For the Fe–22.5% Ni–4% Mn alloy Korenko [8] observed the existence of a C-curve behavior which is typical of the isothermal martensitic transformation in the Fe–Ni–Mn alloy system. The nose temperature for 0.3% martensite formed was around −120°C for a magnetic field of 140 KOe applied for 30 s. Without an additional driving force the transformation is very sluggish by holding at any temperature.

Figure 8 shows martensite volume fraction transformed at a tensile pulse stress of 2 GPa as a function of temperature for tensile pulse durations of 0.2, 0.4, 0.6 and 1.4 μs. These quantitative data give important information on the time dependence (in the microsecond region) of the isothermal martensitic transformation in Fe–22.5% Ni–4% Mn alloy, over the temperature range studied. The amount of martensite transformed is increased with decrease in temperature and, as expected, with increasing tensile pulse duration. No C-curve kinetic behavior of the transformation appears within the experimental range of temperatures between −60 and −177°C; the transformation behaves isothermally like Fe–Ni(–C) alloys. These results are comparable to those of

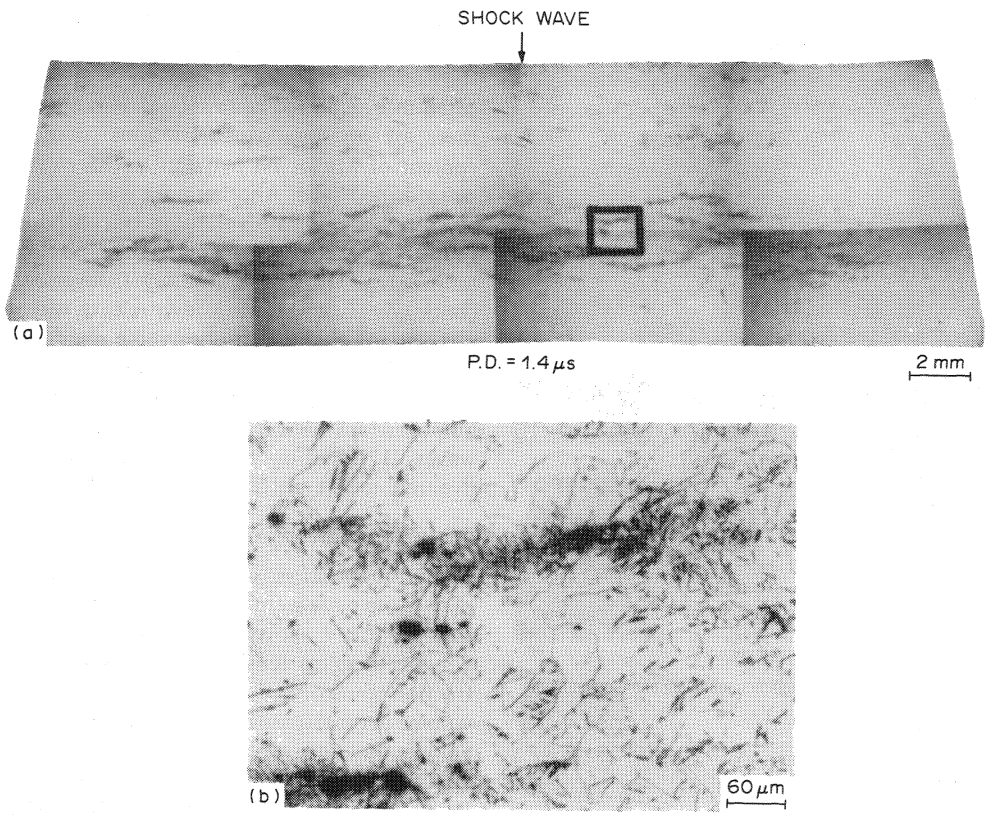

Fig. 5. (a) Micrograph of cross-section of recovered specimen at −100°C and 2 GPa; (b) Magnified micrograph of the framed area in (a).

Malinen *et al.* [20] who investigated Fe–23.6% Ni–(3.3 and 3.6)% Mn alloys applying a pulse field of 400 and 360 KOe, respectively.

The average length of martensite plate formed under the imposed experimental conditions was observed to be $15 \pm 3\ \mu m$. There is not much deviation in the plate length formed under these conditions. The growth rate of martensite plate may not be dependent upon the temperature of pulse duration. This leads to the conclusion that the pulse durations are sufficient for the full growth of the plate, once nucleation occurs. In this sense the number of initially existing and autocatalytically produced nuclei increase with increasing pulse duration and decreasing temperature.

3.3.2. Determination of activation energy. Pati and Cohen's [21] approach for transformation kinetics was used to determine the activation energy, ΔW_a. Assuming that the mean volume, $\bar{V}$, of martensite plate is constant with volume fraction transformed, Pati and Cohen's [21] formulation can be rewritten as

$$\frac{df}{dt} = (P\bar{V} - 1)\left\{f - \frac{n_i \bar{V}}{1 - P\bar{V}}\right\} \times (1 - f)\, \nu \exp\frac{-\Delta W_a}{RT} \quad (1)$$

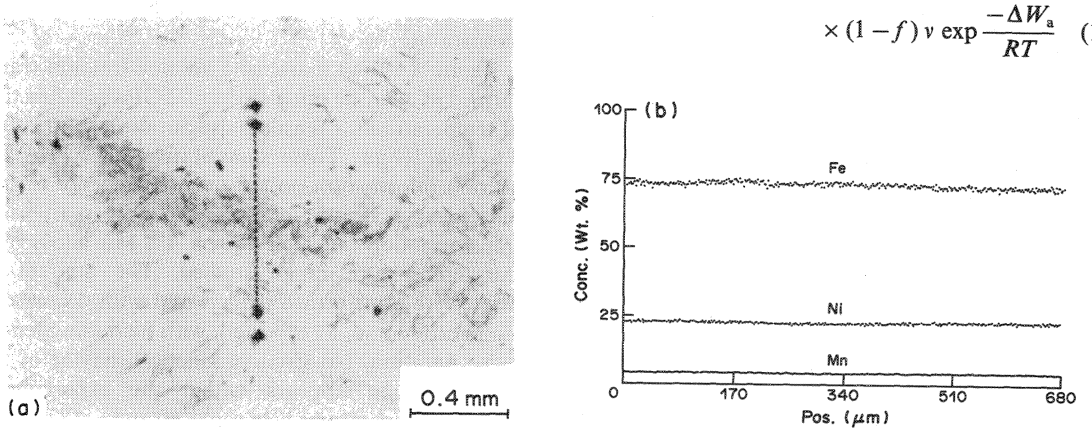

Fig. 6. (a) Magnified micrograph of an area in Fig. 5(a); (b) electron probe microanalysis along the dotted line in (a).

Table 1. Gas-gun operating conditions and results

Operated temperature (°C)	Specimen thickness (mm)	Impact velocity (m/s)	Stress level (GPa)	Pulse duration ($\times 10^{-6}$ s)	Results % martensite
−100	3.8†	168	1.7	0.6	Little spall
−100	3.8†	253	2.5	0.6	Spall
−100	3.8†	318	3.2	0.6	Spall
−60	3.8	193	2.0	0.6	2.0 ± 1.0
−80	9.0	201	2.0	1.4	15.3 ± 5.9
−80	3.8	196	2.0	0.6	36.3 ± 9.6
−80	2.5	200	2.0	0.4	6.5 ± 4.7
−80	1.2	202	2.0	0.2	2.7 ± 1.2
−100	9.0	199	2.0	1.4	29.7 ± 12.2
−100	3.8	198	2.0	0.6	23.7 ± 7.8
−100	2.5	200	2.0	0.4	7.5 ± 3.8
−100	1.2	200	2.0	0.2	5.6 ± 3.3
−110	3.8	201	2.0	0.6	41.3 ± 11.5
−120	9.0	202	2.0	1.4	68.7 ± 3.0
−120	3.8	200	2.0	0.6	51.2 ± 9.4
−120	2.5	198	2.0	0.4	27.0 ± 3.0
−120	1.2	201	2.0	0.2	22.0 ± 5.9
−140	9.0	203	2.0	1.4	80.3 ± 5.2
−140	2.5	201	2.0	0.4	42.3 ± 14.3
−140	1.2	202	2.0	0.2	33.3 ± 11.4
−160	1.2	201	2.0	0.2	41.5 ± 7.1
−177	2.5	194	2.0	0.2‡	44.6 ± 11.8

†Specimens for preliminary shots.
‡Flyer plate of 0.6 mm thickness was used.

where f is the volume fraction of martensite formed at time t, $\bar{V}$ is the mean volume of martensite plate, ΔW_a is the activation energy for nucleation at a given temperature, v is the attempt frequency, n_i is the initial number of embryos, P is the autocatalytic factor, and T is the absolute temperature. Although there are some inherent assumptions in Pati and Cohen's [21] formalism, such as a single activation energy for all nucleation sites and random nucleation events, one can determine the effective activation energy for nucleation operation during the entire course of isothermal transformation [22]. The vibrational frequency, v, is often taken to be equal to the lattice vibrational frequency, $10^{13}\,s^{-1}$. However, Magee [23] suggested that the actual attempt frequency could be much lower if the kinetics of nucleation is controlled by dislocation motion. If we consider v to be equal to the vibrational frequency of the martensite-austenite interface in the embryo, then it could be as low as $10^7\,s^{-1}$.

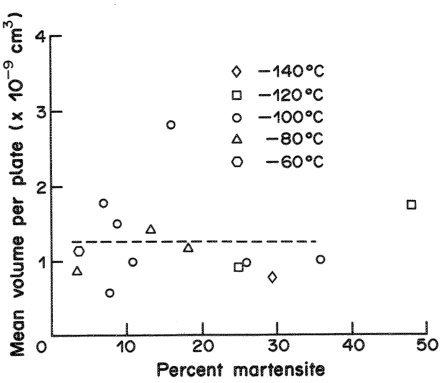

Fig. 7. Average volume of martensite plate as a function of martensite volume fraction transformed.

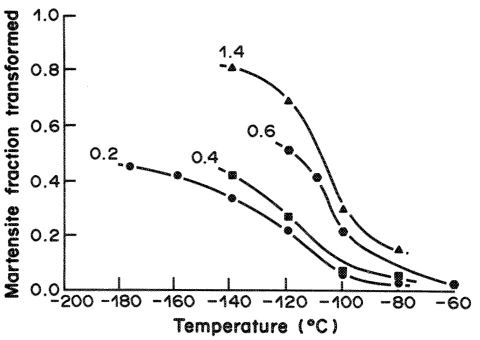

Fig. 8. Martensite volume fraction transformed at tensile stress pulse of 2 GPa as a function of temperature, at different pulse durations of 0.2, 0.4, 0.6 and 1.4 μs.

Integrating equation (1) by using the method of separation of variables, a linear equation is obtained as a function of time,

$$F = At + B \tag{2}$$

where

$$F = \ln\left[\frac{f + \dfrac{n_i \bar{V}}{P\bar{V} - 1}}{f - 1}\right]$$

$$A = (n_i \bar{V} + P\bar{V} - 1)\, v \exp\frac{-\Delta W_a}{RT}$$

$$B = \ln\left[\frac{n_i \bar{V}}{P\bar{V} - 1}\right]$$

By substituting experimental values of fraction (f) versus time (t) at constant temperature, along with values of v, n_i, R and $\bar{V}$ into equation (2), the activation energy, ΔW_a, was computed. Using the least squares method, ΔW_a was iteratively determined by the value of P which gives the minimum root mean square error. In this computation the following

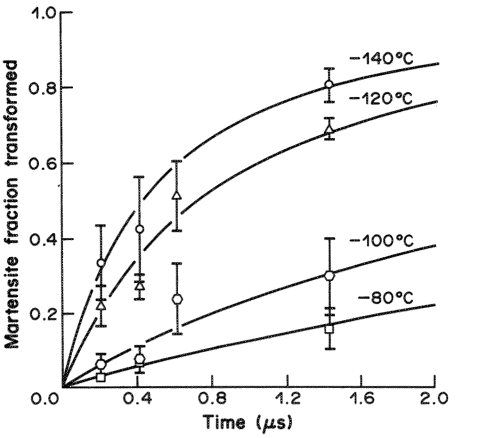

Fig. 9. Experimental points and calculated curves for martensite volume fraction as a function of pulse duration, at different temperatures.

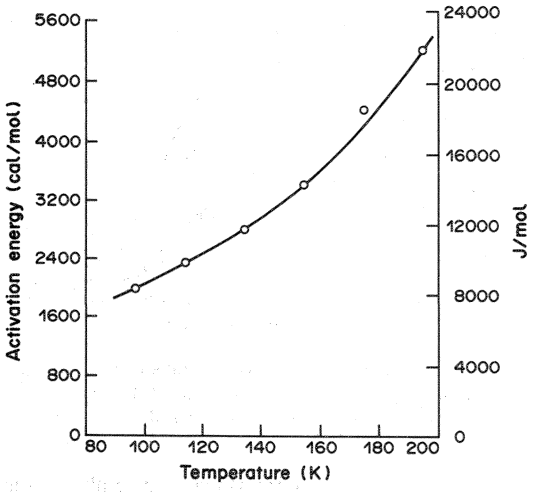

Fig. 10. Activation energy dependence of temperature.

values of n_i and ν were used:

n_i, the initial number of nucleation sites, is $10^7\,cm^{-3}$. This value is most widely used in the kinetic calculations of martensitic transformations.

ν, the lattice vibrational frequency, is $10^{13}\,s^{-1}$, and was chosen to maintain consistency with previous kinetic calculations.

The martensite fraction transformed as a function of time in the present work is shown in Fig. 9. The calculated solid curves [based on equation (1)] for the martensite fraction transformed with time at constant temperatures of −80, −100, −120 and −140°C are in good agreement with the experimental points. All curves in Fig. 9 show an increase in fraction transformed as time is increased; in contrast, the curves for Fe–32% Ni–0.035% C alloy [1] showed a plateau after ~1 μs. This difference in behavior is a consequence of the difference in the nature of the transformation in the two alloys. In the Fe–22.5% Ni–4% Mn alloys the transformation is considered isothermal, while the transformation in Fe–32% Ni–0.035% C alloy is athermal, reaching saturation levels with 1 μs.

It is shown in Fig. 10 that the activation energy decreases with decreasing temperature, which is well-known for isothermal martensitic transformations. This is because the rate of isothermal martensitic transformation is controlled by the nucleation rather than by the growth rate. Neither nucleation nor growth involves diffusion; diffusion-controlled processes have an activation energy that does not depend on temperature. The underlying mechanisms for nucleation, that controls the rate of transformation and establishes the temperature dependence of the activation energy, are not understood yet. The magnitude of the activation energy for the formation of martensite at an applied tensile pulse of 2 GPa is relatively low compared with other experimental results [8, 19], being responsible for the very rapid-isothermal transformation rates in Fe–22.5% Ni–4% Mn alloy. The values of activation energy and autocatalytic factors computed are shown in Table 2.

Table 2. Autocatalytic factors and energetics for Fe–22.5% Ni–4% Mn alloy

Temperature (°C)	Auto-catalytic factor (+10⁸)	Activation energy (ergs/event) (×10⁻¹³)	Chemical driving force (J/mol)	Total driving force (ergs/cm³) (×10⁹)
−177	—	1.372†	−1599.8	−2.577
−160	—	1.635†	−1582.3	−2.554
−140	7.81	2.001	−1552.2	−2.504
−120	7.81	2.422	−1511.4	−2.444
−100	7.80	3.084	−1459.9	−2.368
−80	7.80	3.647	−1398.2	−2.278

†Calculated from one value of f vs t.

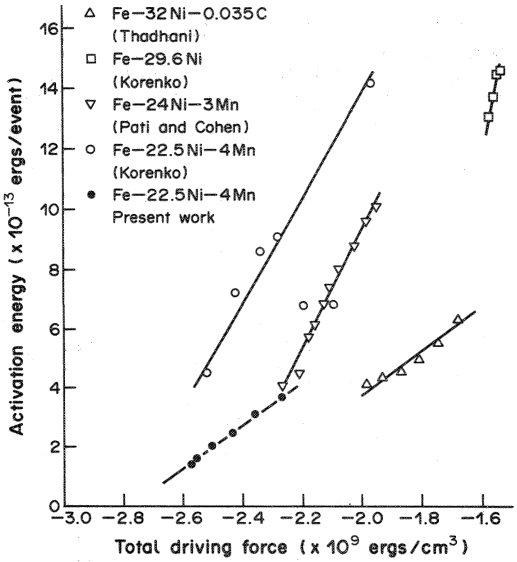

Fig. 11. Relationship between actiation energy and total driving force; Fe–32% Ni–0.035% C [1], Fe–22.5% Ni–4% Mn [8], Fe–29.6% Ni [8], Fe–24% Ni–3% Mn [21].

3.3.3. Mechanical driving force by tensile stress pulse. The martensite morphology in Fe–22.5% Ni–4% Mn alloy induced by a tensile pulse of 2 GPa

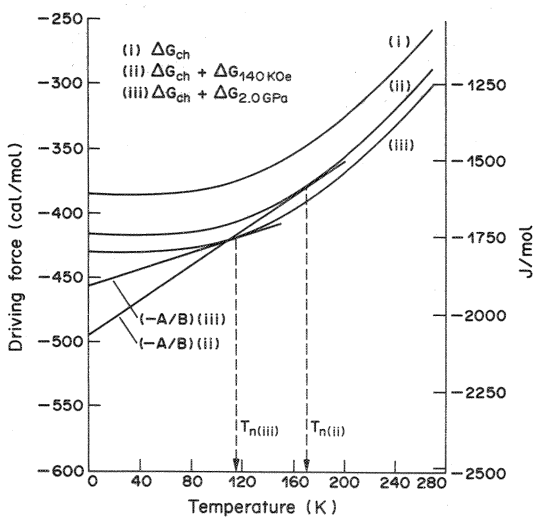

Fig. 12. Kinetic relations for isothermal martensitic transformation in Fe–22.5% Ni–4% Mn alloy.

is plate-like which is evidence of the elastic-stress-assisted martensite. Thus, the tensile pulse can be assumed to be purely elastic. In the elastic regime the M_S temperature change in ferrous alloys is proportional to the applied mechanical stress [24] that contributes a mechanical work term to the overall thermodynamic driving force for the transformation [6]. Since there is no obvious M_S temperature in Fe–22.5% Ni–4% Mn alloy, it is difficult to obtain the mechanical work contribution to the overall driving force. Thadhani and Meyers [1] used the change in M_S temperature as a measure of the mechanical work contribution due to the tensile stress pulse, based on Patel and Cohen's [5] rationalization. The M_S temperature of that alloy changed from -61°C under ambient conditions to -8°C, giving a net M_S change of 53°C with the application of a tensile pulse of 1.4 GPa. Extrapolating the M_S temperature change for a tensile pressure pulse of 2.0 GPa (present work), one obtains an equivalent M_S change of 75.7°C. Since all experiments performed were similar to those in Thadhani and Meyers' work [1], the M_S change of 75.7°C was used to obtain the mechanical work contribution, adopting Patel and Cohen's rationalization expressed by

$$W = \frac{\mathrm{d}\Delta G_{ch}}{\mathrm{d}T}\Delta M_S \tag{3}$$

The value of $\mathrm{d}\Delta G_{ch}/\mathrm{d}T$ within the temperature range of interest (-60 to -177°C) is 2.33 J/mol K. This gives a mechanical work contribution of 176.4 J/mol, due to the tensile pulse of 2.0 GPa.

3.3.4. Transformation energetics. The total driving force, which is the summation of mechanical work and chemical free energy change, is shown in Table 2. The chemical free energy change for martensitic transformation in the Fe–22.5% Ni–4% Mn alloy can be expressed as [8]:

$$\Delta G_{ch} = 1613.7 + 5.56 \times 10^{-3} T^2 - 8.83 \times 10^{-5} T^3 + 15.22 \times 10^{-8} T^4 \text{ (J/mol)} \tag{4}$$

Figure 11 shows the activation energy linearly related to the total driving force for different Fe–Ni–Mn and Fe–Ni–C alloys reported in the literature. The curve for the Fe–22.5% Ni–4% Mn alloy (present work) lies towards the bottom, directly below Pati and Cohen's Fe–24% Ni–3% Mn alloy [21], and reveals a lower slope, compared to other alloys. The linear relationship for the Fe–22.5% Ni–4% Mn alloy studied in this investigation can be given as

$$\Delta W_a = 2.1 \times 10^{-19} + 7.585 \times 10^{-29}\Delta G_{tot} \text{ (J/event)} \tag{5}$$

The ΔW_A vs ΔG_{tot} functional relationship for Fe–22.5% Ni–4% Mn alloy induced by a magnetic field of 140 KOe [8] is

$$\Delta W_a = 3.42 \times 10^{-19} + 11.4 \times 10^{-29}\Delta G_{tot} \text{ (J/event)} \tag{6}$$

This linear relationship between ΔW_a and ΔG is expressed, in a general form, as: $\Delta W_a = \mathrm{A} + \mathrm{B}\Delta G$. Applying this equation to Pati and Cohen's [21] kinetic equation, one can obtain the equation

$$\Delta G(\dot{f}) = \frac{-A}{B} + \left(\frac{R}{B}\ln\frac{\dot{F}}{n\bar{V}v}\right)T \tag{7}$$

The intersections of the lines expressed by equation (7) with the chemical free energy change ΔG vs T curve give the transformation rates as a function of temperature. Using equation (7) and the known constant values of A and B, one can predict the peak (nose) temperature of C-curve kinetics for the isothermal martensitic transformation. Figure 12 shows ΔG vs T plots for Fe–22.5% Ni–4% Mn alloy transformed by (i) cooling, (ii) application of magnetic field of 140 KOe and (iii) application of mechanical work by tensile stress pulse of 2 GPa. The "nose" temperature, T_n, of the C-curve in this plot can be predicted from the maximum transformation rate, $\dot{f}$, for both the present investigation and Korenko's work [8]. The ΔG_{ch} vs T curves are obtained from equation (4). Olson and Cohen [25] explain how the kinetics of the transformation ($\dot{f}$) is obtained as a function of temperature from the intersections of the straight lines starting at point $-A/B$ on the ΔG axis. This procedure is applied to obtain the "nose" temperature in Fig. 12. Curve (i) is given by equation (4). Curve (ii) has the driving force due to the magnetic field added to it, while curve (iii) has the driving force due to the tensile pulse added to the chemical free energy. The point at which the line with intercept $-A/B$ tangentiates the ΔG_{tot} vs T curve gives the temperature (T_n) at which the transformation rate is maximum. T_n can be expressed as

$$1613.7 - 5.56 \times 10^{-3} T_n^2 + 17.66 \times 10^{-5} T_n^3 + 45.7 \times 10^{-8} T_n^4 = -\Delta G_{app} + \frac{A}{B} \text{ (J/mol)} \tag{8}$$

where ΔG_{app} is the applied driving force. Thus, T_n varies with ΔG_{app} as well as with the A/B ratio.

The experimental peak temperature, T_n, for Fe–22.5% Ni–4% Mn alloy at 140 KOe was reported to be -120 ± 5°C, while the value calculated from equation (8) is -103°C. T_n at a tensile pulse of 2.0 GPa is computed to be -156°C. Without any applied force, T_n for the Fe–22.5% Ni–4% Mn alloy is around -140°C according to the empirical correlations of peak temperature vs percent Mn [26]. Thus, due to the increasing amount of additional driving force, the peak temperature increases first, and then decreases.

Both Thadhani and Meyers [1] and the present results show lower slopes in the activation energy vs driving force curves. While the position of the line in the plot (Fig. 11) can be changed by the assumptions made in the calculational procedures for the fraction transformed, the slopes would not be affected. The coefficient B, which is the slope ($\partial\Delta W_a/\partial\Delta G$) of the curve in Fig. 11, corresponds to the activation volume

V^* (volume transformed/event divided by atomic volume of a b.c.c. unit cell). The lower slope yields the lower activation volume. The physical interpretation of the activation volume, V^*, is, according to Magee [23, 27], the volume of the embryo at nucleation (peak of ΔG vs volume of martensite curve). The activation volume represents the critical step for a martensite embryo to be a martensite plate. The value of activation energy is proportional to this activation volume; the activation volumes compared to those reported by other investigations in bulk Fe–Ni–Mn alloys are the following:

65 Ω present investigation
100 Ω Korenko [8]
190 Ω Pati and Cohen [21]

where Ω is the atomic volume. The lower activation volume results from the transformation at the higher applied force. This decrease in the activation volume at the high driving forces imparted by the tensile pulses is consistent with the trends postulated by Olson and Cohen [28] and expressed by

$$\left(\frac{\Delta Q}{\Delta Q_0}\right)^q = 1 - \left(\frac{\Delta G}{\Delta G_0}\right)^p \qquad (9)$$

where ΔQ_0 is the maximum activation energy, ΔG_0 is the threshold driving force, and p and q describe the long-range and short-range behaviors of the interface (assumed to be composed of a regular array of dislocations). It is qualitatively seen that, for $1 < p$, $q < 0$, the change in slope of equation (9) follows the same trend as the one shown in Fig. 11. The physical underpinnings of equation (9) are that nucleation is controlled by motion of the austenite–martensite (embryo) interface, consisting of discrete dislocation arrays. This motion is opposed by short- and long-range obstacles interacting with the individual dislocations.

It is noted that there is a critical applied driving force (ΔG_{cr}) for Fe–Ni–Mn alloys which either moves the peak temperature to very low temperatures (less than liquid nitrogen temperature) or results in a non C-curve kinetic behavior similar to that observed in Fe–Ni and Fe–Ni–C alloys. The curvature of $\Delta G_{ch}(T)$ shown in Fig. 12 is related to the C-curve behavior in isothermal martensitic transformations in Fe–22.5% Ni–4% Mn alloys where the maximum nucleation rate generally occurs in the vicinity of −120 to −170°C. For an applied force (ΔG_{app}) less than ΔG_{cr}, the "nose" may shift to higher values than the nose temperature at zero-applied stress. Increasing the magnitude of ΔG_{app}, the nose temperature may continue to increase until it reaches the temperature at which the magnitude of $\Delta G_{ch}(T)$ is dramatically increased. However, in the case that ΔG_{app} is larger than ΔG_{cr}, the nose temperature may decrease very much. By decreasing temperature gradually close to 0 K, the shear stress opposing the movement of the nucleation interface in the alloy increases, but the value of the free energy change becomes steady. Unfortunately, it was not possible to conduct gas-gun experiments at lower than liquid nitrogen temperature. In order to confirm the existence of the nose temperature of the transformation it would be necessary to perform experiments at very low (less than −196°C) temperature with a high applied driving force.

3.4. *Morphology and crystallography*

3.4.1. Optical micrography. The plate morphologies of the thermally induced and tensile-pulse-assisted martensite are shown in Figs 13(a) and 13(b), respectively. The thermally induced martensite in Fig. 13(a) is similar to the structure observed by Kajiwara [29, 30] in an Fe–22.9% Ni–3.8% Mn alloy. According to him a large martensite plate with a macroscopic $(225)_f$ habit plane consists of small fragmentary plates (subplates) having $(112)_f$ habit plane, after removing surface layers. On the other hand, the tensile-pulse-assisted martensite, shown in Fig. 13(b), was observed to be more plate-like with a clear mid-rib formed at a pulse duration of 1.4 μs.

Figure 14(a) shows martensite plates induced by tensile stress pulse and the traces of slip lines resulting from indentation in a grain. This morphology is typically obtained in the temperature range of −60 to −160°C. Martensite plates do independently form and grow. The four slip traces induced by the

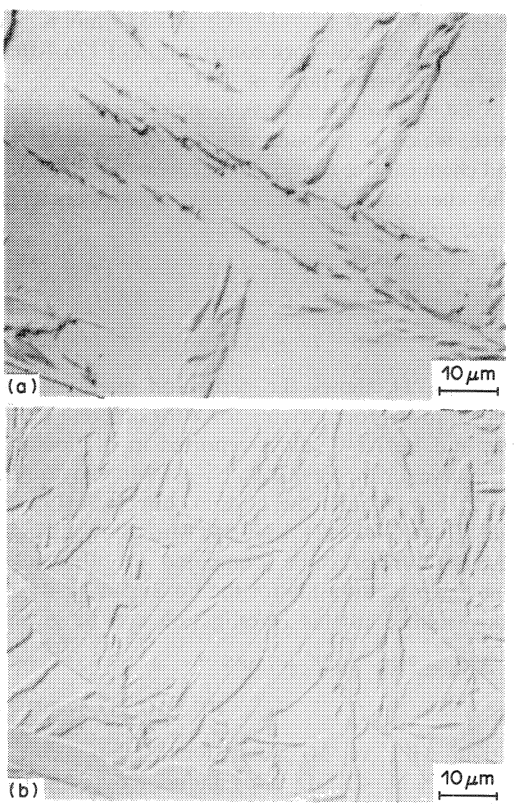

Fig. 13. (a) Morphology of thermally induced martensite after removal of the surface of specimen exposed to liquid nitrogen for 24 h; (b) Morphology of stress-assisted martensite formed in specimen impacted at −100°C and 2 GPa.

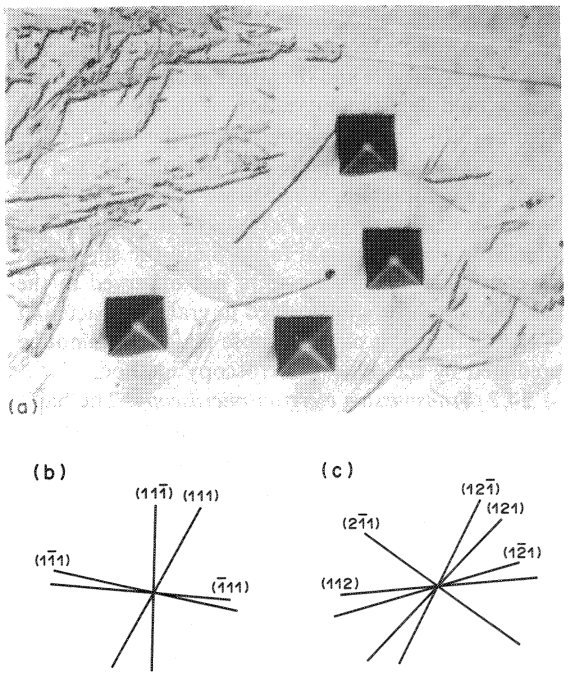

Fig. 14. (a) Tensile pulse induced martensite and traces produced by identation in a grain ($[\bar{3}\ 5\ 15]_f$ normal); (b) slip traces and their calculated indices, (c) habit plane traces of martensite plates, and their calculated indices.

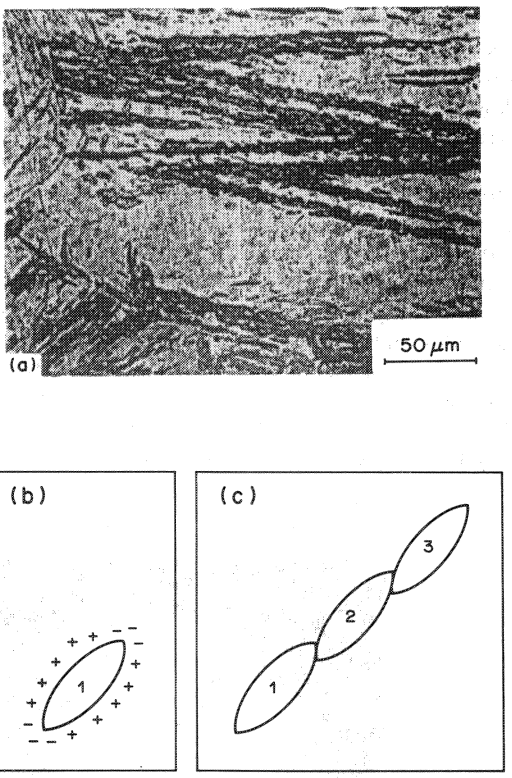

Fig. 15. (a) Optical micrograph of martensite induced by tensile stress pulse of 2 GPa at −177°C; (b) hydrostatic stresses imposed by formation of a plate; "+" and "−" indicate compression and tension, respectively; (c) sequence of platelet formation.

indenter are shown in Fig. 14(b). The indices of habit plane traces of each martensite plate [in Fig. 14(c)] were calculated and identified to be $\{1\ 1\ 2\}_f$. The calculated grain normal was $[\bar{3}\ 5\ 15]_f$ for Fig. 14(a); an additional grain was calculated and the normal was $[\bar{5}\ 14\ 29]_f$.

In contrast to thermally nucleated martensite, martensite plates consisting of small subplates do not appear in the impacted specimens. Instead, the subplates (which have (112) habit plane) nucleate and directly grow in the direction of their habit planes without establishing the macroscopic habit plane (225). The time to nucleate and grow a martensite plate is less than one microsecond, with a large amount of driving force provided at the impact moment. The driving force to accommodate the plastic deformation due to the transformation is sufficient to trigger the individual martensite (112) plates, and make them grow to their maximum size without being along a (225) plane.

At lower temperature, −177°C, small plates cluster together to form long and narrow plates, shown in Fig. 15(a). The plates so formed are relatively narrow and the interface with austenite phase is rough, meaning that the driving force is large enough to trigger nucleation, but the flow stress of austenite itself is already too high to allow the nucleus to grow fully in the radial direction. The morphology of the martensite induced by the tensile stress pulse at −177°C is similar to that transformed at −196°C

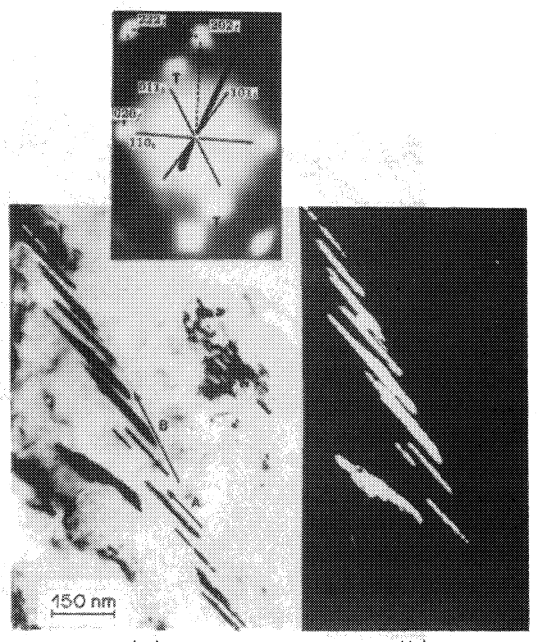

Fig. 16. (a) Transmission electron micrograph showing a group of twins inside martensite transformed at −140°C and 2 GPa; (b) dark field image of twins on $(112)_b$ plane; (c) and (d) stereographic analyses for habit (in f.c.c.) and twin (in b.c.c.) planes, respectively.

without any driving force, seen in Fig. 13(a). Thus, one may conclude that the growth of martensite is governed by the flow stress of the parent phase. This flow stress increases very significantly at low temperature. Kajiwara [31, 32] determined the flow stress as a function of temperature for Fe–26% Ni–3.8% Mn alloy. The flow stress of this alloy exponentially increases from 90 MPa at room temperature to 210 MPa at liquid nitrogen temperature.

If the plastic deformation due to the transformation is easily accommodated in the alloy, then the subplates directly grow in the radial direction from the (112) habit plane, upon nucleation. However, if it is hard to accommodate the plastic deformation, the subplates having a (112) habit plane may undergo very limited growth. Additional transformation thus takes place by nucleation of new platelets. These platelets would nucleate at a position that is energetically favourable and the stress assist from the first plate would help the nucleation of the second plate. Figure 15(b) shows, schematically, the hydrostatic stresses imposed by a plate. The regions marked by "+" are compressed, while those marked by "−" are under tension. Figure 15(c) shows the sequence in which the platelets would form. Since the slip traces developed by indentation were not observed in the case of martensite transformed in grains impacted at −177°C, the habit plane of those plates could not be predicted by the optical microscopy method.

3.4.2. Transmission electron microscopy. The habit plane (112) of the individual martensite subplates, shown by Yang *et al.* [33], rotated in an Fe–21%

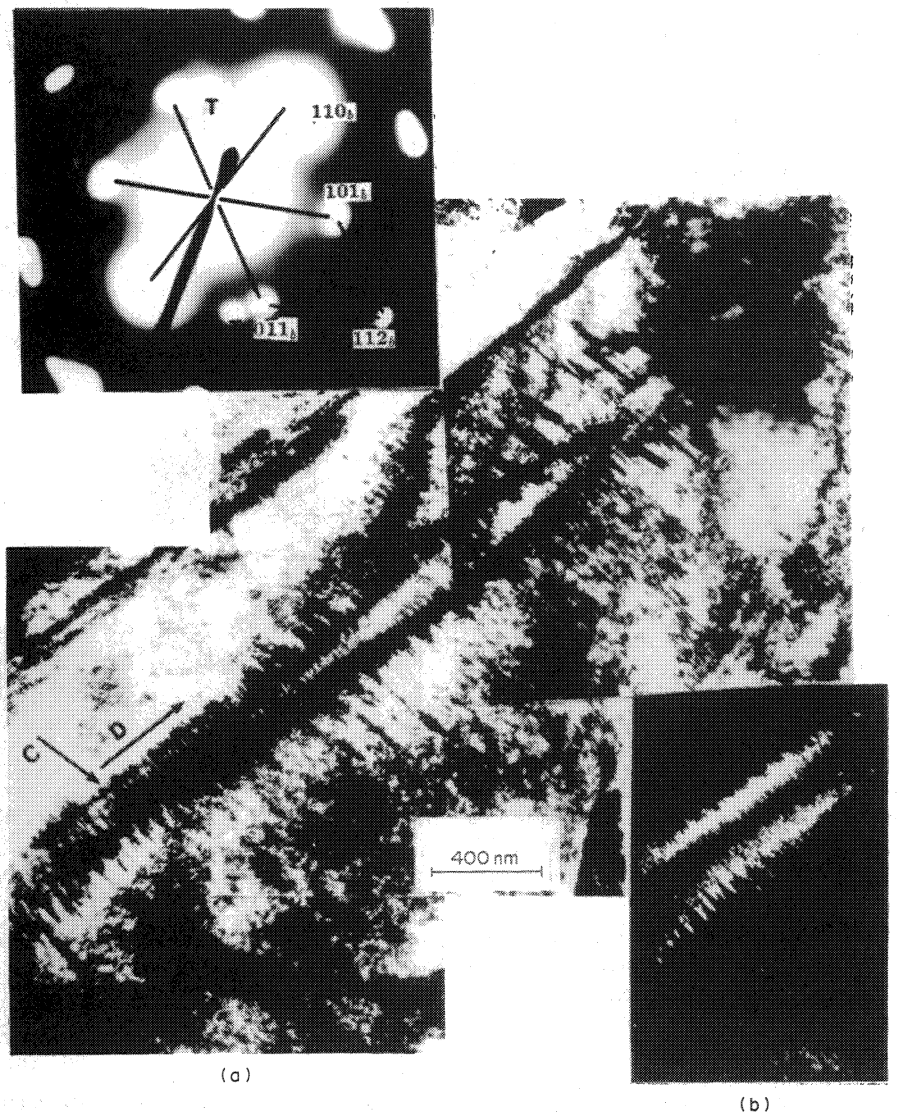

Fig. 17. (a) Transmission electron micrograph showing a twinned martensite (bottom left) and unidentified feature (top right) surrounded by a group of martensite twins; (b) dark field image of twins [bottom left (a)], taken using twin reflection shown in diffraction pattern.

Ni–4% Mn alloy, during the growth of thermally induced martensites. The tensile-pulse-induced martensite in ferrous alloy systems had not previously been characterized crystallographically. Transmission electron microscopic observation of tensile-pulse-induced martensite was conducted in order to determine the orientation of the martensite plates.

Figure 16(a) is a bright field transmission electron micrograph showing a group of twins (indicated in direction A) initially formed along the habit plane (B) at -140°C and at a tensile stress pulse of 2.0 GPa. The diffraction pattern shows that the foil orientation is $[\bar{1}\,0\,1]_f//[\bar{1}\,\bar{1}\,1]_b$, and that the direction of the habit plane (indicated by B) is parallel to $[1\,1\,1]_f$ and $[0\,1\,1]_b$. The dark field image in Fig. 16(b), taken using a twin reflection, shows twins on $(11\bar{2})_b$ plane. By stereographic analysis it was found that the habit plane in f.c.c. is $(\bar{1}12)_f$ and the twin plane in b.c.c. is $(11\bar{2})_b$. From the above observations and analysis, Kurdjumov–Sachs (K-S) orientation relations are found to be $(111)_f//(011)_b$ and $[\bar{1}\,0\,1]_f//(\bar{1}\,\bar{1}\,1)_b$.

Figure 17(a) shows another example of the martensile formed at the tensile stress pulse of 2.0 GPa. The diffraction pattern, that only shows martensite reflections, indicates that the foil orientation is $[1\,1\,\bar{1}]_b$. The surface trace C is parallel to $[1\,\bar{2}\,3]_b$. Applying K-S relations for the stereographic analysis, the surface trace D turns out to be $(\bar{1}02)_b$ which is parallel to $(\bar{1}12)_f$. Figure 17(b) shows the corresponding dark field image using twin reflection.

4. CONCLUSIONS

(1) Tensile pulses developed in the interior of the Fe–22.5% Ni–4% Mn alloy by the reflection of shock waves at free surfaces induce martensitic transformation.

(2) The martensite transformed is localized in a specific region within the maximum pulse duration zone in the interior of the alloy, due to the discontinuity of the shock wave interactions.

(3) A very rapid-isothermal martensitic transformation occurs in this alloy system, with the fraction transformed increasing with pulse duration. No isothermal C-curve kinetics was observed in the temperature range of -60 to -177°C; instead, the transformation rate increased with decreasing temperature.

(4) The activation energies of martensitic transformation in the alloy were calculated using Pati and Cohen's kinetic model. The values, which are lower than those determined in any other isothermal martensite experiments, decrease with decreasing temperature and are linearly related to the total driving force.

(5) The temperature for maximum transformation rate ("nose" temperature of C-curve) depends on the magnitude of the applied driving force and was calculated to be -156°C for a 2.0 GPa tensile pulse. A linear relationship between the activation energy and total driving force was found. From this relationship, the activation volume for nucleation was calculated to be equal to 65 atomic volumes.

(6) Martensite plates with clear mid-ribs are often formed in the stress-pulse loaded specimens, while the thermally induced martensite (at -196°C) is much more fragmented.

(7) The habit plane of martensite transformed was numerically computed to be $\{1\,1\,2\}_f$ by measuring angles between habit plane orientations on a grain, of which the normal was determined from slip traces formed by indentations on the grain.

(8) The habit plane observed by transmission electron microscopy is also $(112)_f$. The $(112)_b$ twins start forming along this habit plane.

Acknowledgements—The authors express their great appreciation to the following persons: Mr D. C. Erlich and the SRI-International staff for conducting the gas-gun experiments; Dr N. N. Thadhani, CETR, for performing the transmission electron microscopy and for invaluable discussions; Dr A. D. Romig Jr, Sandia National Laboratories, for providing assistance with electron microprobe analysis of the alloy and for valuable criticism and suggestions; Drs D. Matlock and E. Brown, Colorado School of Mines, for their kind assistance in hot-rolling; Dr G. B. Olson, Massachusetts Institute of Technology, for supplying the alloy used in this investigation; Drs K. P. Staudhammer, Los Alamos National Laboratory, and M. Yoshida, Japan National Chemical Laboratory for Industry for helpful discussions; Dr P.-A. Persson, CETR, for his financial support to finalize this investigation; Mr L. H. Yu for experimental help.

This research program was funded by the National Science Foundation under Grant No. DMR 81-15127 and by the New Mexico Department of Economic Development and Tourism through the Center for Explosives Technology Research.

REFERENCES

1. N. N. Thadhani and M. A. Meyers, *Acta metall.* **34,** 1625 (1986).
2. E. Sheil, *Z. anorg. Chem.* **207,** 21 (1932).
3. A. W. McReynolds, *J. appl. Phys.* **20,** 896 (1949).
4. S. A. Kulin, M. Cohen and B. L. Averbach, *Trans. Am. Inst. Min. Engrs* **192,** 661 (1952).
5. J. R. Patel and M. Cohen, *Acta metall.* **1,** 531 (1953).
6. M. A. Meyers and J. R. C. Guimaraes, *Mater. Sci. Engng* **24,** 289 (1976).
7. E. O. Snell, J. C. Shyne and A. Goldberg, *Metallography* **10,** 299 (1977).
8. M. K. Korenko, D.Sc Thesis, Massachusetts Institute of Technology (1973).
9. M. K. Korenko and M. Cohen, in *Proc. Int. Conf. Martensitic Transformations, ICOMAT-1979*, p. 388. M.I.T. Press, Cambridge, Mass. (1979).
10. N. N. Thadhani, Ph.D Thesis, New Mexico Institute of Mining and Technology (1984).
11. R. T. DeHoff and F. N. Rhines, *Quantitative Microscopy*, p. 52. McGraw-Hill, New York (1968).
12. R. L. Fullman, *Trans. Am. Inst. Min. Engrs* **197,** 447 (1953).
13. H.-r. Pak, S. N. Chang and M. Kato, *J. Mater. Sci.* **20,** 947 (1985).
14. L. M. Barker, Research Report SC-RR-67 143, Sandia Corporation, Albuquerque, New Mexico (April 1967).
15. C. L. Mader and M. S. Shaw, LA-7264, Los Alamos Scientific Laboratory, Los Alamos, New Mexico (1978).

16. R. G. McQueen and S. P. Marsh, *J. geophys. Res.* **71,** 1751 (1966).
17. D. E. Grady, *J. geophys. Res.* **85,** 913 (1980).
18. D. A. Shockey, J. F. Kalthoff and D. C. Erlich, *Int. J. Fract.* **22,** 217 (1983).
19. S. R. Pati and M. Cohen, *Acta metall.* **17,** 189 (1969).
20. P. A. Malinen, V. D. Sadovskiy and I. P. Sorokin, *Phys. metals Metallogr.* **24,** 101 (1967).
21. S. R. Pati and M. Cohen, *Acta metall.* **19,** 1327 (1971).
22. M. Cohen and C. M. Wayman, in *Metallurgical Treatises* (edited by J. K. Tien and J. F. Elliot), p. 445. Am. Inst. Min. Metall. Petrol. Engrs (1981).
23. C. L. Magee, in *Phase Transformations*, p. 115. American Society of Metals (1970).
24. G. B. Olson and M. Cohen,m *J. less-common Metals* **28,** 107 (1972).
25. G. B. Olson and M. Cohen, *Metall. Trans.* **13A,** 1907 (1982).
26. C. H. Shih, B. L. Averbach and M. Cohen, *Trans. Am. Inst. Min. Engrs* **202,** 183 (1955).
27. C. L. Magee, *Metall. Trans.* **2,** 2419 (1971).
28. G. B. Olson and M. Cohen, in *Frontiers in Materials Technologies* (edited by M. A. Mayers and O. T. Inal), p. 43, North Holland, Amsterdam (1984).
29. S. Kajiwara, in *Proc. Int. Conf. Martensitic Transformations, ICOMAT-1979*, p. 362. M.I.T. Press, Cambridge, Mass. (1979).
30. S. Kajiwara, *Phil. Mag.* **A43,** 1483 (1981).
31. S. Kajiwara, *J. Phys. Suppl.* **43,** c4–97 (1982).
32. S. Kajiwara, *Acta metall.* **32,** 407 (1984).
33. D. Z. Yang, B. P. J. Sandvik and C. M. Wayman, *Metall. Trans.* **15A,** 1555 (1984).